Ignition and formation dynamics of a polariton condensate on a semiconductor microcavity pillar

C. Antón,[1,2] D. Solnyshkov,[3] G. Tosi,[1] M. D. Martín,[1,2] Z. Hatzopoulos,[4,5] G. Deligeorgis,[4] P. G. Savvidis,[4,6] G. Malpuech,[3] and L. Viña[1,2,7,*]

[1]*Departamento de Física de Materiales, Universidad Autónoma de Madrid, Madrid 28049, Spain*
[2]*Instituto de Ciencia de Materiales "Nicolás Cabrera", Universidad Autónoma de Madrid, Madrid 28049, Spain*
[3]*Institut Pascal, PHOTON-N2, Clermont Université, Blaise Pascal University, CNRS, 24 avenue des Landais, 63177 Aubière Cedex, France*
[4]*FORTH-IESL, P.O. Box 1385, 71110 Heraklion, Crete, Greece*
[5]*Department of Physics, University of Crete, 71003 Heraklion, Crete, Greece*
[6]*Department of Materials Science and Technology, University of Crete, 71003 Heraklion, Crete, Greece*
[7]*Instituto de Física de la Materia Condensada, Universidad Autónoma de Madrid, Madrid 28049, Spain*
(Received 22 May 2014; revised manuscript received 19 September 2014; published 17 October 2014)

We present an experimental study on the ignition and decay of a polariton optical parametric oscillator (OPO) in a semiconductor microcavity pillar. The combination of a continuous-wave laser pump, under quasi-phase-matching conditions, and a nonresonant, 2-ps-long pulse probe allows us to obtain the full dynamics of the system. The arrival of the probe induces a blueshift in the polariton emission, bringing the OPO process into resonance with the pump, which triggers the OPO process. We time-resolve the polariton OPO signal emission for more than 1 ns in both real space and momentum space. We fully characterize the emission of the OPO signal with spectral tomography techniques. Our interpretations are backed up by theoretical simulations based on the two-dimensional coupled Gross-Pitaevskii equation for excitons and photons.

DOI: 10.1103/PhysRevB.90.155311 PACS number(s): 67.10.Jn, 78.47.jd, 78.67.De, 71.36.+c

I. INTRODUCTION

Exciton-polaritons in semiconductor microcavities (MCs), when injected with a *pump* laser close to the inflection point of the lower polariton branch (LPB) dispersion, undergo a nonlinear process above a pump power threshold. Carrier-carrier interactions self-stimulate a coherent scattering from the pump state into *signal* and *idler* polariton states, whose frequency and in-plane momentum fulfill phase-matching conditions. The signal state population, generated by this optical parametric oscillator (OPO) [1–4] process, reaches occupation values above 1, exhibiting a new form of nonequilibrium superfluid behavior [5], metastability of quantum vortices [6,7], and persistence of currents [8–10].

Lateral etching of planar MCs has been successfully exploited for the creation of a large variety of new geometries: the resulting discretization of the energy spectrum opens an interesting scenario of different OPO phase-matching conditions in one- (1D) and zero-dimensional (0D) MCs. In the former case, the 1D discretization of the LPB in several energy subbands yields the opportunity to obtain exotic intra- and interbranch OPO processes [11–14]. Furthermore, interesting studies of the second-order coherence of both signal and idler states have been performed recently [15]. In the latter case (0D OPO polaritons), although the most common excitation scheme for micropillars is nonresonant excitation, [16–20] different groups have reported the possibility to induce a parametric oscillation between discrete energy states: from the initial injected energy mode to two neighboring signal and idler states. [21–23]

In this work, we study a 40-μm-$\varnothing$ pillar MC, which is sufficiently large to neglect the 0D confinement effects, but it still has a bounded spatial extension where polaritons cannot propagate large distances. We excite the sample using a *pump-probe* excitation scheme that differs from common resonant excitation [1–4,24]. We ignite a long-lived OPO polariton signal and observe a transient behavior, characterized by a collective oscillation of the condensed OPO polaritons in the pillar. Thereafter, they reach a quasisteady state, displaying a ringlike emission pattern due to repulsive interaction with the exciton population in the center of the pillar [25]. The OPO signal is switched on with the pulsed *probe* at the exciton energy level which blueshifts the LPB, making the *continuous-wave* (cw) pump enter in resonance conditions in a OPO process that lives for $\sim$1 ns. We study the full dynamics of the creation and decay of this confined OPO condensate in real space and momentum space (**k** space). The interpretation of the experimental measurements of the spatial emission dynamics is supported by theoretical simulations using the 2D coupled Gross-Pitaevskii equations for excitons and photons.

II. SAMPLE AND EXPERIMENTAL SETUP

We investigate a high-quality $5\lambda/2$ AlGaAs-based MC with 12 embedded quantum wells and a Rabi splitting $\Omega_R = 9$ meV. Further information about this sample is given in Ref. [26]. Pillars with different diameters have been sculpted through reactive ion etching. We have chosen a 40-μm-$\varnothing$ pillar in an area of the sample where the detuning is close to zero [27]. Figure 1 shows a scanning electron microscopy image of such a pillar, including the excitation scheme.

The sample, mounted in a cold-finger cryostat and kept at 10 K, is excited with pump and probe laser beams under the following conditions. For the continuous-wave experiments (Sec. III A), we use only a pump beam obtained from a cw Ti:Al_2O_3 laser. It is tuned at $E_p = 1.5416$ eV, impinging on the sample with an in-plane momentum $(\mathbf{k}_p)_x = -1.9\ \mu\text{m}^{-1}$, fulfilling the phase-matching conditions $2E_p = E_s + E_i$ and $2\mathbf{k}_p = \mathbf{k}_s + \mathbf{k}_i$ [where the subindex s (i) means signal (idler)].

*luis.vina@uam.es

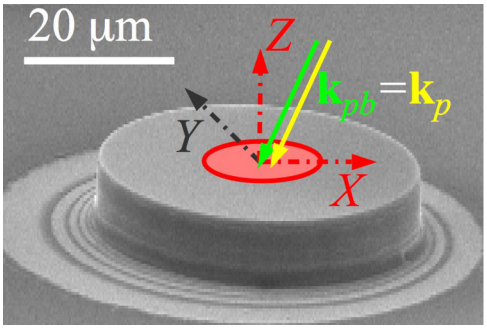

FIG. 1. (Color online) Scanning electron microscopy image of a 40-μm-$\varnothing$ pillar with the pump-probe excitation scheme: the solid arrows, contained in the XZ plane, sketch the beams directions, $\mathbf{k}_{pb}$ and $\mathbf{k}_p$, impinging at the center of the pillar. Three dot-dashed arrows define the coordinates' origin chosen for the experiments.

Its power is set to $P_p = 160$ mW. For the time-resolved experiments (Secs. III B and III C), the excitation scheme is represented in Fig. 2. In this case the cw pump beam is out of OPO phase-matching conditions since now its energy is tuned slightly above the LPB ($E_p = 1.5419$ eV). The second excitation source, the probe, is a pulsed Ti:Al_2O_3 laser (2-ps-long pulses); it is tuned into resonance with the exciton mode ($E_{pb} = 1.5445$ eV), and its power, $P_{pb} = 230$ mW, is strong enough to trigger the OPO process together with the pump. The origin of time $t = 0$ is set to the instant when the probe impinges on the pillar. The two excitonic lines labeled X_1 and X_2 originate from excitons uncoupled to the cavity modes due to slight quantum well thickness variations (of the order of a monolayer) between different quantum wells.

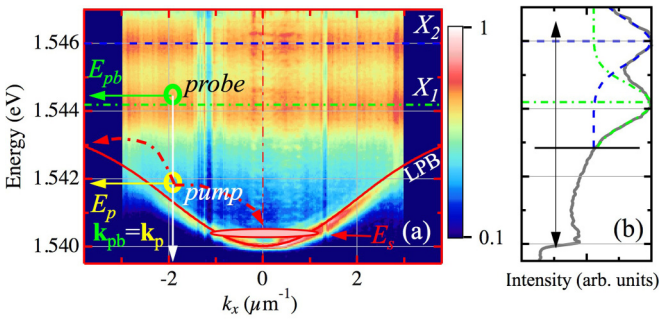

FIG. 2. (Color online) (a) Experimental LPB dispersion obtained under nonresonant (1.612 eV), weak-excitation conditions; the overlapping thin solid curve is a guide to the eye. The horizontal dot-dashed and dashed lines mark the energies 1.544 and 1.546 eV of excitons $\mathbf{X_1}$ and $\mathbf{X_2}$, respectively. The energies, E_p and E_{pb}, and momenta, $\mathbf{k}_p$ and $\mathbf{k}_{pb}$, of the pump and probe, respectively, are marked with circles and left-pointing arrows. Dot-dashed arrows depict the OPO process that yields the OPO signal at E_s and $\mathbf{k}_s \approx 0$, marked with an elongated circle. The PL is coded in a false, normalized, logarithmic color scale. (b) Spectrum emission integrated in $\mathbf{k}$ space depicted as a solid line. The two bare exciton levels are obtained with a double-Gaussian fit: the dot-dashed (dashed) horizontal line marks the energy of the maximum PL emitted by the X_1 (X_2) exciton. A horizontal solid line schematically separates, at 1.543 eV, the spectra that correspond to excitons (above, upward-pointing arrow) and polaritons (below, downward-pointing arrow) in the pillar.

Further information about the origin of the exciton emission is given in Ref. [25].

For the experimental results described in Sec. III, the laser beams are focused on the sample through a high-numerical-aperture (0.6) lens, forming two overlapping elliptically shaped spots [10-μm-$\varnothing$ (20-μm-$\varnothing$) minor (major) axis along the Y (X) axis] impinging on the pillar with an in-plane momentum $\mathbf{k}_{p/pb} = \{(\mathbf{k}_{p/pb})_x, (\mathbf{k}_{p/pb})_y\} = \{-1.9, 0\}$ μm^{-1} (see the solid arrows in Fig. 1). The same lens is used to collect and direct the emission towards a 0.5-m spectrometer coupled to a CCD (Sec. III A) and a streak camera (Secs. III B and III C). The photoluminescence (PL) can be resolved in the near field (real space) as well as in the far field ($\mathbf{k}$ space). The distribution of polaritons in $\mathbf{k}$ space is accessed by imaging the Fourier plane of the lens used to collect the PL, taking advantage of the direct relation between the angle of emission and the in-plane momentum of polaritons [28]. To avoid the direct reflection of the pump and probe beams, we block the emission in $\mathbf{k}$ space for $|\mathbf{k}| > 1.5$ μm^{-1}, and we spectrally filter the polariton PL with an energy detection range of 1 meV around 1.54 eV. The lens that focuses the real- or $\mathbf{k}$-space PL distribution into the spectrometer entrance slit is displaced laterally by discrete steps, yielding a tomographic reconstruction of energy- and time-resolved images.

III. EXPERIMENTAL RESULTS AND DISCUSSION

This section compiles the results of cw and time-resolved experiments in the pillar, which are organized as follows. In Sec. III A we address the tomographic spectral distribution of polaritons in the pillar under cw OPO excitation, in both real space and $\mathbf{k}$ space. In Sec. III B we study the dynamics of the polariton emission under pump-probe excitation. In this case, the cw pump laser beam is out of OPO conditions (slightly blue detuned from the LPB); only after the arrival of the probe is the induced blueshift of the LPB large enough to start the OPO process. In Sec. III C, for the sake of completeness, we present the polariton dynamics with only the probe excitation, where the decay of the polariton PL is faster and limited by the relaxation dynamics from photogenerated excitons towards the polariton ground state.

A. The cw spectroscopy characterization of OPO signal emission

Figure 3 summarizes the spectral tomography of the polariton emission in both real space and $\mathbf{k}$ space under a cw pump excitation. The OPO signal energy is $E_s \approx 1.54$ eV, with a full width $\Delta E_s \approx 0.8$ meV. Figure 3(a) [Fig. 3(e)] shows the polariton emission in real space (Y) [$\mathbf{k}$ space (k_y)] at the central $X = 0$ ($k_x = 0$) cross section. Since the pump is impinging at the center of the pillar, the polariton emission displays a ringlike distribution, which can be seen in the cross section in Fig. 3(a), where the emission is spatially enclosed in the area $5 < |\mathbf{r}| < 15$ μm. Figure 3(e) shows that polaritons are static at low energies ($\sim$1.5398 eV) since their emission is confined at $\mathbf{k} \sim 0$, and they spread in a disk with a radius $|\mathbf{k}| < 1.2$ μm^{-1} at slightly higher energies ($\sim$1.540 eV).

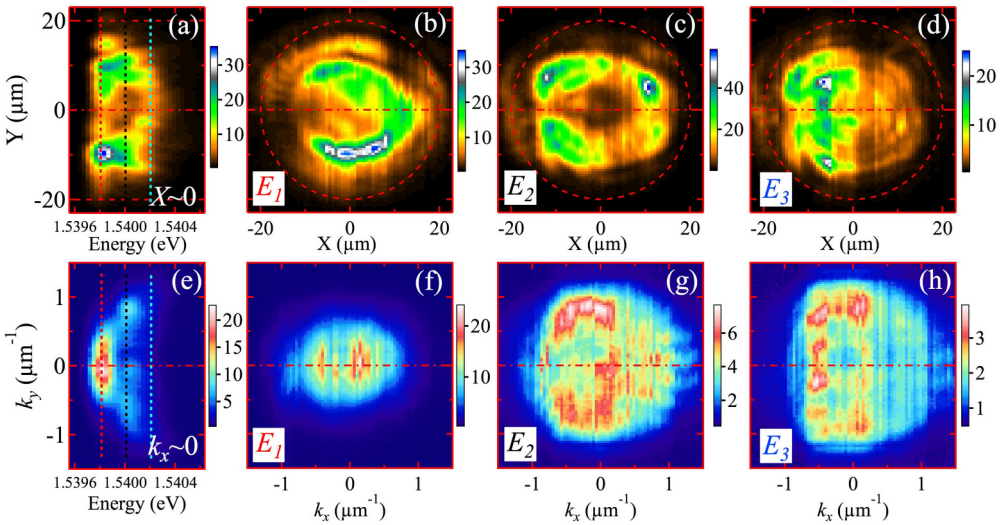

FIG. 3. (Color online) (a) Real-space and (e) momentum-space polariton spectrum emission at the $X = 0$ and $k_x = 0$ cross sections in the pillar, respectively. The three dashed vertical lines mark the positions where the full X-Y and k_x-k_y PL maps have been reconstructed in (b)–(d) and (f)–(h), respectively. The three selected energies are $E_1 = 1.5398$ eV, $E_2 = 1.5400$ eV, and $E_3 = 1.5402$ eV. In (b)–(d) dashed red circles mark the limits of the pillar. The PL maps are coded in linear, false-color scales.

We perform a two-dimensional reconstruction of the spectrum emission, showing the full X-Y and k_x-k_y PL distributions of polaritons at three selected energies, $E_1 = 1.5398$ eV, $E_2 = 1.5400$ eV, and $E_3 = 1.5402$ eV, in Figs. 3(b)–3(d) and 3(f)–3(h), respectively. Figure 3(b) reveals the ringlike distribution of polaritons at E_1. The angle of incidence of the pump creates an asymmetrical blueshift in the left side of the pillar due to polariton propagation, so the polariton ring-shaped emission is broken in the region $\{x, y\} = \{-10, 0\}$ μm. At a higher energy, E_2 [Fig. 3(c)], polaritons emit from a ring with a radius of 10 μm with a smaller side gap. Figure 3(d) shows an almost flat disk of emission, whose radius is $\sim$15 μm.

In **k** space, Fig. 3(f) shows a small disk (radius of 0.7 μm^{-1}) in the polariton distribution. This demonstrates that polaritons lying at low energy (E_1), which are distributed along the ring in Fig. 3(b), are confined in real space, with a small amount of kinetic energy. The confinement of polaritons at E_1 is also hinted at in the momentum cross section in Fig. 3(e). Figures 3(g) and 3(h) evidence a flat distribution in momentum space, where polaritons have all possible values of momenta inside a disk of radius $|\mathbf{k}| < 1$ and 1.5 μm^{-1}, respectively. For energies higher than E_3, polariton emission is distributed in a ring (not shown) corresponding to a cloud of uncondensed, hot polaritons in the LPB.

B. Igniting a long-lived OPO process with a probe-induced blueshift

In this section we show how the OPO process is triggered by the arrival of a probe beam. Moreover, through real-space measurements, we reveal the ring-shaped distribution of signal polaritons, and analyzing **k**-space images, we characterize their movement around the pillar.

The pump (cw) plus probe (pulsed) excitation configuration activates a long-lived stimulated OPO scattering process. The time during which the OPO is active is much longer than the photon lifetime, which is estimated from the Q factor to be $\sim$10 ps. The real- and **k**-space dynamics of the signal emission are presented in Figs. 4 and 5, respectively. In these

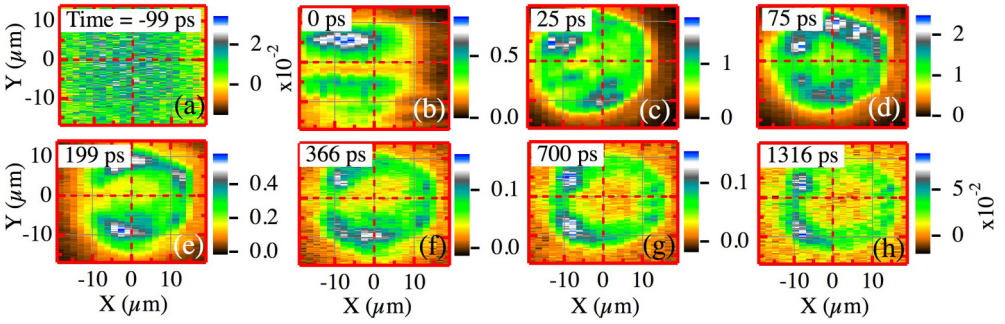

FIG. 4. (Color online) Real-space polariton emission dynamics in the pillar under pump and probe beam excitation. The time is shown by the labels in each panel. The time $t = 0$ coincides with the arrival of the probe. The PL is coded in a linear, false-color scale that is shown to the right of each panel. The complete X-Y polariton emission dynamics is available in the Supplemental Material [29].

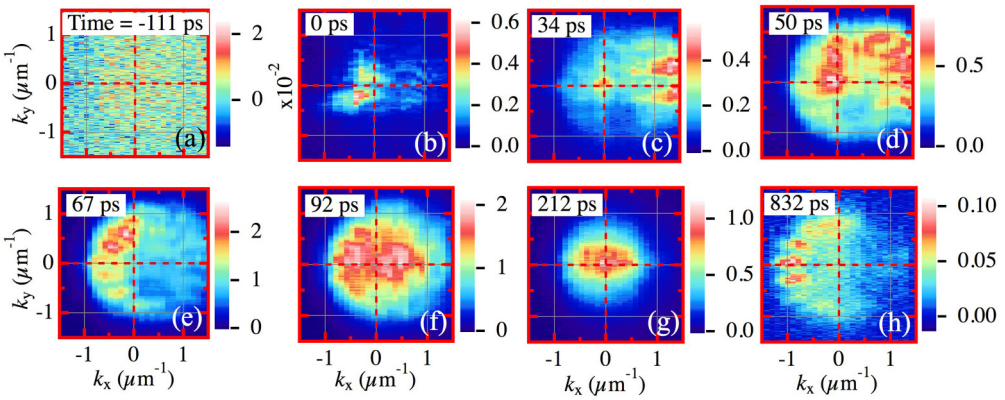

FIG. 5. (Color online) Momentum-space polariton emission dynamics in the pillar. The excitation conditions are the same as in Fig. 4. The time is shown by the labels in each panel. The PL is coded in a linear, false-color scale shown to the right of each panel. The complete k_X-k_Y polariton emission dynamics is available in the Supplemental Material [29].

time-resolved experiments, the energy resolution is similar to that of the energy width of the OPO signal ΔE_s.

Figure 4 compiles two-dimensional images of the polariton signal emission at different times in real space. For each panel, the time is displayed in the top left corner, with the temporal origin set at the instant when the probe impinges on the sample. Figure 4(a) shows that, before the arrival of the probe pulse ($t = -99$ ps), there is no signal emission since the pump is off of phase-matching conditions. At $t = 0$ [Fig. 4(b)], the probe impinges on the pillar; the spot shape is distorted due to the fact that $\mathbf{k}_{pb} \neq 0$. The polariton emission rapidly arises from the whole pillar surface, which is seen as a flat homogeneous disk [Fig. 4(c)]. The PL increases for ∼100 ps, as shown in Fig. 4(d); thereafter, the extra population of polaritons induced by the probe decreases. When the OPO process has switched on, the polariton dispersion becomes ring shaped [Fig. 4(e)]: the real-space polariton distribution resembles that shown in Fig. 3(c). Polaritons emit close to the border of the pillar due to the blueshift induced by the cw pump. This polariton emission persists for more than ∼1 ns [see Figs. 4(f)–4(h)].

Figure 5 shows the dynamics in **k** space of the polariton population. As observed in real space, there is no OPO signal emission before the arrival of the probe [Fig. 5(a)]. The pulsed probe arrives at the pillar at $t = 0$ [Fig. 5(b)]; the spurious emission from $\mathbf{k} \sim 0$ is unfiltered scattered laser light. The probe creates an extra polariton population around $\mathbf{k} = \{-1.5,0\}$ μm^{-1} that rapidly moves in the $+k_x$ direction (not shown here; see the movie in the Supplemental Material [29]). At $t = 34$ ps [Fig. 5(c)], the population has moved towards $\mathbf{k} = \{1.5,0\}$ μm^{-1}. Figure 5(d) shows that, at $t = 50$ ps, the polariton emission is homogeneously distributed in a disk of radius $|\mathbf{k}| \approx 1$ μm^{-1}. At $t = 67$ ps [Fig. 5(e)], the population reverts its angle of emission towards $-k_x$. As mentioned for Fig. 4, ∼100 ps after the arrival of the probe, its induced extra population weakens, and the OPO signal is redistributed at the center of **k** space [Fig. 5(f)]. The oscillations arise from the probe-injected excitons, which are excited with a certain angle. The relaxation of excitons yields polaritons that possess a nonzero momentum. As clearly inferred from the dynamics of the **k**-space distribution, polaritons change their initial momentum due to several bounces against the MC wall. The gain follows the injected probe distribution as it moves within the pillar, until the excitonic population dies off and a more stable, switched-on OPO process takes place, which resembles the polariton distributions in real space and **k** space shown in Fig. 3. For longer times, $t = 212$ ps [Fig. 5(g)], the emission is mainly perpendicular to the sample surface, i.e., at $\mathbf{k} \approx 0$. At later times [Fig. 5(h)], two effects are observed: first, there is a lobelike structure at $\mathbf{k} = \{1.0,0\}$ μm^{-1}, and second, there is a progressive decay of the central ($\mathbf{k} = 0$) population. The latter effect is due to the fact that the emission energy is redshifting with time and we have not been following this redshift with the streak camera since its energy detection is fixed for these experiments.

C. Nonresonant excitation with solely a pulsed probe

In this section, for completeness, we address the polariton dynamics obtained when only the pulsed probe beam excites the pillar. The polariton emission dynamics in real space and **k** space are summarized in Figs. 6(a)–6(d) and 6(e)–6(h), respectively. Figure 6(a) shows the absence of emission before the arrival of the probe. Figures 6(b) and 6(c) show the switching on of the polariton emission, following a dynamics similar to that shown in Fig. 4, during the first ∼100 ps. Figure 6(d) demonstrates the shorter lifetime of the polariton population created under these excitation conditions; after ∼250 ps, the polariton PL has disappeared.

In a similar fashion, Figs. 6(e)–6(h) show the dynamics of the emission in **k** space. An oscillation of the polariton momentum similar to that described in Figs. 5(c)–5(e) is obtained here during the first ∼100 ps. The polariton emission moves in the k_x direction, going from -1.5 to $+1.5$ μm^{-1} in ∼70 ps. At later times [Fig. 6(g)], the emission originates from $k \approx 0$, and for $t = 355$ ps, the lack of emission is confirmed [Fig. 6(h)].

D. Comparison of the dynamics of the two excitation schemes involving a probe

The dynamics of the spatially integrated emission buildup is depicted in Fig. 7. A similar behavior is obtained for

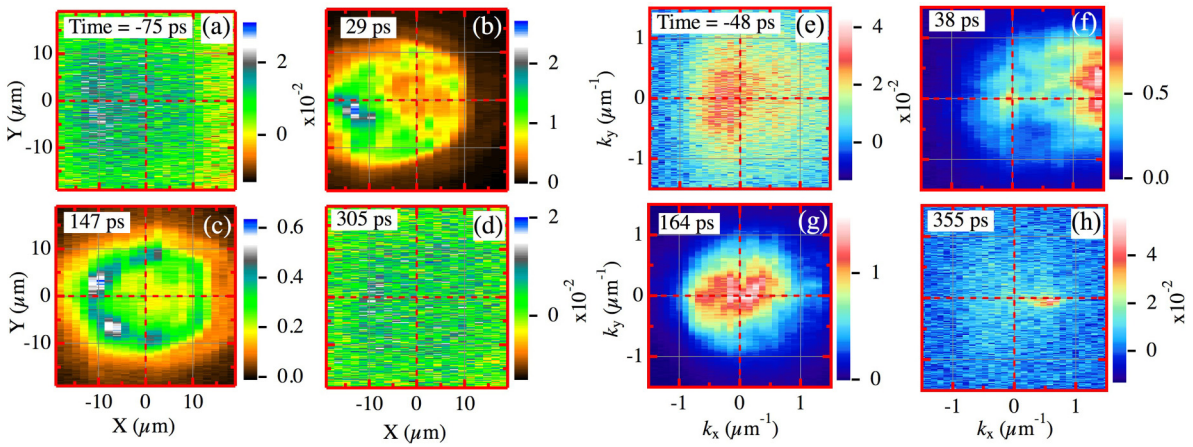

FIG. 6. (Color online) (a)–(d) Real-space and (e)–(h) **k**-space polariton emission distributions in the pillar. The time is shown by the labels in each panel. Only the probe beam excites at the center of the pillar. The time $t = 0$ coincides with the arrival of the probe. The PL is coded in a linear, false-color scale shown to the right of each panel. The complete X-Y and k_X-k_Y polariton emission dynamics are available in the Supplemental Material [29].

pump-probe (blue line) and probe-only (orange line) excitation conditions. The PL reaches its maximum emission ∼50 ps after the probe is gone. It is on the decay dynamics that differences between the two excitation conditions appear. Under probe-only excitation we observe a monoexponential decay of the PL, with a characteristic decay time of 63 ps. The decay is markedly different in the presence of the out-of-resonance pump. In this case, the PL decay is biexponential, with a fast decay time of 76 ps and a long-lived polariton population lasting more than 1 ns, evidenced by the slow (∼500 ps) decay time.

IV. THEORETICAL DESCRIPTION

To model our experimental results under the OPO configuration, described in Sec. III B, we make use of the 2D coupled Gross-Pitaevskii equations for photons $\psi(x,y)$ [Eq. (1)] and excitons $\varphi(x,y)$ [Eq. (2)]:

$$i\hbar\frac{\partial\psi}{\partial t} = -\frac{\hbar^2}{2m_{ph}}\Delta\psi + \frac{\hbar\Omega_R}{2}\varphi + U\psi - \frac{i\hbar}{2\tau_{ph}}\psi + P + P_X + f, \quad (1)$$

$$i\hbar\frac{\partial\varphi}{\partial t} = -\frac{\hbar^2}{2m_X}\Delta\varphi + \frac{\hbar\Omega_R}{2}\psi + \alpha_1|\varphi|^2\varphi + U\varphi. \quad (2)$$

Here, $m_{ph} = 4\times10^{-5}m_0$ is the photon mass, $m_X = 0.6m_0$ is the exciton mass (m_0 is the free electron mass), $\hbar\Omega_R = 9$ meV is the Rabi splitting, and $\alpha_1 = 6E_b a_B^2$ is the triplet interaction constant [30] ($E_b = 10$ meV is the exciton binding energy, and $a_B = 10$ nm is the exciton Bohr radius).

The confinement potential of the pillar, acting on the photonic and excitonic parts, is described by U. $\tau_{ph} = 1$ ps is the photon lifetime (the exciton decay is neglected), P is the quasiresonant pumping term, exciting the system at a given frequency and in-plane momentum (the same values as in the experiments), blue detuned with respect to the polariton branch, and f is the noise, which serves to account for the effects of spontaneous scattering. The cw pumping provides an average of 10 particles in a unit cell of $h = 0.25$ μm in the steady state, while the spontaneous scattering creates 0.01 particle. To describe the nonresonant probe, we use a pulsed pumping term P_X, tuned at the exciton resonance, with the same duration and wave vector as in the experiments. No disorder potential was taken into account because its effects were not observed in the experiments.

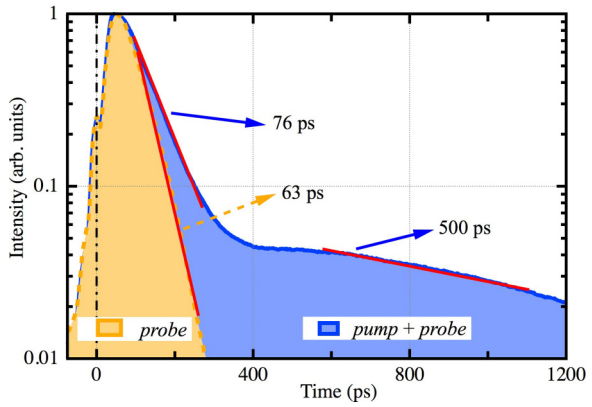

FIG. 7. (Color online) Dynamics of the integrated polariton PL under the two excitation conditions: pump plus probe (solid line) and probe only (dashed line). Straight solid lines are included in the different exponential decays as guides to the eye. PL is plotted on a logarithmic axis.

The results of the theoretical simulations are presented in Fig. 8. We plot the spatial distribution of the PL from the MC for the signal state by applying a filter in **k** space, blocking the emission for $\mathbf{k} > 1.5$ μm^{-1} as in the experiments. This spatial distribution is plotted at two different instants in order to demonstrate the agreement between experiment and theory. Figures 8(a) (25-ps delay) and 8(b) (400-ps delay) should be compared with Figs. 4(c) and 4(g), respectively.

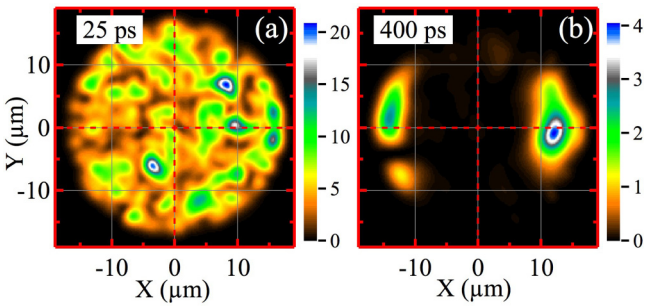

FIG. 8. (Color online) Real-space polariton emission dynamics in the pillar under pump and probe beam excitation: (a) 25 and (b) 400 ps after the probe excitation. The PL is coded in a linear, false-color scale.

First of all, the main conclusion is that in both experiment and theory the creation of excitons by the probe laser leads to a blueshift of the polariton dispersion, which moves it into resonance with the pump laser. The density of the pump state then becomes sufficient to start OPO scattering into the signal and idler states.

Because of the hysteresis of the polariton system in the bistable regime, the pump density remains high even when the probe excitons have decayed through relaxation and emission from strongly photonic states. The OPO regime persists for more than 1 ns, much longer than the characteristic decay times in the system. The presence of the confinement potential of the pillar prevents the escape of the signal polaritons under the influence of the potential of the pump, contributing to the persistence of the OPO. The decay of the OPO is due to the overall imbalance between pumping and losses. The small difference between pumping and losses becomes more and more important because the decrease of the total polariton density leads to a redshift of the pumped mode, bringing it out of OPO resonance, decreasing the efficiency of pumping even further. This is evidenced in the experiments by the fact that the time evolution of the intensity becomes a concave function of time (the effective lifetime becomes progressively shorter at longer times). In the simulations, increasing the pumping allows us to overcome this decay and to maintain a permanently stable OPO regime. However, one should note that in the bistable configurations, the presence of noise (spontaneous scattering) leads to spontaneous transitions between the two stable solutions at long time scales. This noise also contributes to driving the system towards the low-intensity state and to switching off the OPO.

More conclusions can be drawn from the spatial shape of the signal at different moments of time, which results from the interplay of several effects. At initial moments of time, the density becomes sufficient to surpass the OPO threshold everywhere in the pillar, with a large spreading in the reciprocal space caused by different phase-matching conditions (different signal wave vectors and energies) at different points because of the nonhomogeneous pump profile. However, the signal exhibits a homogeneous emission over the whole surface of the pillar, with the rapid spreading of polaritons being caused by the strong interactions between all particles: those created by the pump (after the bistability has been passed) and those injected with the probe. This is well reproduced by the theoretical simulations [Fig. 8(a)]. At later times [Fig. 8(b)], as the total density drops down and the spatial redistribution stabilizes, the signal concentrates around opposite sides of the pillar along the X axis. This is due to the spatial shape of the pump laser, which creates conditions favorable for the OPO at only these points, which are located at the minima between the pump spot and the pillar boundary: the pump density at the center of the pillar is too high to maintain resonant OPO because the signal polaritons are pushed away from the center and their density becomes insufficient there to maintain stable OPO. The overall good agreement between theory and experiment supports our interpretation of the experimental observations.

V. CONCLUSIONS

We have presented experimental conditions to obtain a long-lived polariton condensate in a pillar MC. The process involves two excitation beams impinging at the center of the pillar with the same wave vector: a cw pump, slightly blue detuned from the inflection point of the LPB, and a pulsed probe, resonantly creating excitons. The polariton population created by the arrival of the probe induces a blueshift of the LPB, which enters into resonance with the pump beam, triggering the OPO process. The cw pump keeps on feeding the OPO after the pulsed probe has disappeared because of the hysteresis of the polariton bistability. As a result of the combined effect of both beams, the OPO signal emission lasts for more than 1 ns, much longer than any of the characteristic times of the MC. The polariton condensate dynamics observed when using just the probe beam is remarkably similar to that obtained for the two-beam excitation but is much shorter lived. The exciton population created by the probe beam efficiently relaxes to the LPB and from there follows the OPO dynamics. The characteristic decay time is one order of magnitude shorter than that obtained under the two-beam excitation conditions.

ACKNOWLEDGMENTS

C.A. acknowledges financial support from the Spanish FPU scholarship. P.S. acknowledges the Greek GSRT program "ARISTEIA" (1978) and EU ERC "Polaflow" for financial support. The work was partially supported by the Spanish MEC MAT2011-22997 and EU-FP7 ITN INDEX (289968) projects.

[1] P. G. Savvidis, J. J. Baumberg, R. M. Stevenson, M. S. Skolnick, D. M. Whittaker, and J. S. Roberts, Phys. Rev. Lett. **84**, 1547 (2000).

[2] P. G. Savvidis, J. J. Baumberg, R. M. Stevenson, M. S. Skolnick, D. M. Whittaker, and J. S. Roberts, Phys. Rev. B **62**, R13278 (2000).

[3] J. J. Baumberg, P. G. Savvidis, R. M. Stevenson, A. I. Tartakovskii, M. S. Skolnick, D. M. Whittaker, and J. S. Roberts, Phys. Rev. B **62**, R16247 (2000).
[4] M. Saba, C. Ciuti, J. Bloch, V. Thierry-Mieg, R. Andre, L. S. Dang, S. Kundermann, A. Mura, G. Bongiovanni, J. L. Staehli, and B. Deveaud, Nature (London) **414**, 731 (2001).
[5] A. Amo, D. Sanvitto, F. P. Laussy, D. Ballarini, E. del Valle, M. D. Martín, A. Lemaître, J. Bloch, D. N. Krizhanovskii, M. S. Skolnick, C. Tejedor, and L. Viña, Nature (London) **457**, 291 (2009).
[6] D. N. Krizhanovskii, D. M. Whittaker, R. A. Bradley, K. Guda, D. Sarkar, D. Sanvitto, L. Viña, E. Cerda, P. Santos, K. Biermann, R. Hey, and M. S. Skolnick, Phys. Rev. Lett. **104**, 126402 (2010).
[7] K. Guda, M. Sich, D. Sarkar, P. M. Walker, M. Durska, R. A. Bradley, D. M. Whittaker, M. S. Skolnick, E. A. Cerda-Méndez, P. V. Santos, K. Biermann, R. Hey, and D. N. Krizhanovskii, Phys. Rev. B **87**, 081309 (2013).
[8] D. Sanvitto, F. M. Marchetti, M. H. Szymańska, G. Tosi, M. Baudisch, F. P. Laussy, D. N. Krizhanovskii, M. S. Skolnick, L. Marrucci, A. Lemaître, J. Bloch, C. Tejedor, and L. Viña, Nat. Phys. **6**, 527 (2010).
[9] G. Tosi, F. M. Marchetti, D. Sanvitto, C. Anton, M. H. Szymańska, A. Berceanu, C. Tejedor, L. Marrucci, A. Lemaître, J. Bloch, and L. Viña, Phys. Rev. Lett. **107**, 036401 (2011).
[10] C. Antón, G. Tosi, M. D. Martín, L. Viña, A. Lemaître, and J. Bloch, Opt. Express **20**, 16366 (2012).
[11] G. Dasbach, M. Schwab, M. Bayer, D. N. Krizhanovskii, and A. Forchel, Phys. Rev. B **66**, 201201 (2002).
[12] M. Abbarchi, V. Ardizzone, T. Lecomte, A. Lemaître, I. Sagnes, P. Senellart, J. Bloch, P. Roussignol, and J. Tignon, Phys. Rev. B **83**, 201310(R) (2011).
[13] T. Lecomte, V. Ardizzone, M. Abbarchi, C. Diederichs, A. Miard, A. Lemaître, I. Sagnes, P. Senellart, J. Bloch, C. Delalande, J. Tignon, and P. Roussignol, Phys. Rev. B **87**, 155302 (2013).
[14] J. Cuadra, D. Sarkar, L. Viña, J. M. Hvam, A. Nalitov, D. Solnyshkov, and G. Malpuech, Phys. Rev. B **88**, 235312 (2013).
[15] V. Ardizzone, M. Abbarchi, A. Lemaître, I. Sagnes, P. Senellart, J. Bloch, C. Delalande, J. Tignon, and P. Roussignol, Phys. Rev. B **86**, 041301 (2012).
[16] O. El Daif, A. Baas, T. Guillet, J. P. Brantut, R. I. Kaitouni, J. L. Staehli, F. Morier-Genoud, and B. Deveaud, Appl. Phys. Lett. **88**, 061105 (2006).
[17] D. Bajoni, P. Senellart, E. Wertz, I. Sagnes, A. Miard, A. Lemaître, and J. Bloch, Phys. Rev. Lett. **100**, 047401 (2008).
[18] M. Maragkou, A. J. D. Grundy, E. Wertz, A. Lemaître, I. Sagnes, P. Senellart, J. Bloch, and P. G. Lagoudakis, Phys. Rev. B **81**, 081307(R) (2010).
[19] G. Nardin, T. K. Paraïso, R. Cerna, B. Pietka, Y. Leger, O. El Daif, F. Morier-Genoud, and B. Deveaud-Plédran, Appl. Phys. Lett. **94**, 181103 (2009).
[20] G. Nardin, Y. Léger, B. Pietka, F. Morier-Genoud, and B. Deveaud-Plédran, Phys. Rev. B **82**, 045304 (2010).
[21] G. Dasbach, M. Schwab, M. Bayer, and A. Forchel, Phys. Rev. B **64**, 201309 (2001).
[22] D. Bajoni, E. Peter, P. Senellart, J. L. Smirr, I. Sagnes, A. Lemaître, and J. Bloch, Appl. Phys. Lett. **90**, 051107 (2007).
[23] L. Ferrier, S. Pigeon, E. Wertz, M. Bamba, P. Senellart, I. Sagnes, A. Lemaître, C. Ciuti, and J. Bloch, Appl. Phys. Lett. **97**, 031105 (2010).
[24] D. Ballarini, D. Sanvitto, A. Amo, L. Viña, M. Wouters, I. Carusotto, A. Lemaître, and J. Bloch, Phys. Rev. Lett. **102**, 056402 (2009).
[25] V. K. Kalevich, M. M. Afanasiev, V. A. Lukoshkin, K. V. Kavokin, S. I. Tsintzos, P. G. Savvidis, and A. V. Kavokin, J. Appl. Phys. **115**, 094304 (2014).
[26] P. Tsotsis, P. S. Eldridge, T. Gao, S. I. Tsintzos, Z. Hatzopoulos, and P. G. Savvidis, New J. Phys. **14**, 023060 (2012).
[27] We define the exciton-photon detuning as $\delta = E_C - E_X$, where E_C and E_X are the cavity mode and exciton energy at $\mathbf{k} = 0$, respectively.
[28] M. Richard, J. Kasprzak, R. Romestain, R. André, and L. S. Dang, Phys. Rev. Lett. **94**, 187401 (2005).
[29] See the Supplemental Material at http://link.aps.org/supplemental/10.1103/PhysRevB.90.155311 for movies giving a complete description of the polariton emission dynamics.
[30] M. Vladimirova, S. Cronenberger, D. Scalbert, K. V. Kavokin, A. Miard, A. Lemaître, J. Bloch, D. Solnyshkov, G. Malpuech, and A. V. Kavokin, Phys. Rev. B **82**, 075301 (2010).